Dynamics and stability of the Townsend discharge in nitrogen in narrow gaps

Yu. A. Astrov,* A. N. Lodygin, and L. M. Portsel
Ioffe Physical-Technical Institute, Politekhnicheskaya 26, 194021 St. Petersburg, Russia
(Received 15 May 2013; revised manuscript received 9 February 2014; published 31 March 2014)

This paper investigates the dynamics of the Townsend discharge in nitrogen in narrow gaps. To provide stability of discharge in a broad range of current, we apply a plane-parallel structure, one of the electrodes of which is made of a high-resistivity gallium arsenide. The results of experiments are analyzed in the framework of theory [Yu. P. Raizer *et al.*, Tech. Phys. **51**, 185 (2006)], which considers the dynamics of discharge in short nitrogen-filled gaps of similar structures. According to the theory, a key parameter of discharge dynamics is time ϑ that defines the rate of discharge response to perturbations. In our work, time ϑ is experimentally found by analyzing the noise spectrum of the discharge glow in the stable and spatially uniform state of the structure. This characteristic time depends linearly on the discharge gap width, which corroborates conclusions based on the standard model of Townsend discharge. However, its values are substantially shorter compared to those predicted by theory. The relationship between ϑ and experimentally observed critical current density for the oscillatory instability, j_{cr}, is applied to find the discharge negative differential resistance for a set of parameters of the discharge gap.

DOI: 10.1103/PhysRevE.89.033109 PACS number(s): 52.80.Dy, 05.40.Ca, 52.35.Mw

I. INTRODUCTION

The Townsend discharge is considered the simplest self-sustained mode of discharge in a gas. Under the commonly studied conditions, at the electrode separation d_g of 1 cm and more, the Townsend discharge is observed at current density j not exceeding 1–10 μA/cm^2. The sustaining voltage of such a discharge, U_S, only slightly depends on j and is close to the voltage U_B that initiates discharge in a gas-filled gap [1,2]. The homogeneous stationary state of the discharge becomes unstable at some (critical) value of current. The instability results in the formation of so-called dissipative structures, the dynamics of which can be different. The loss of stability of a Townsend discharge is usually interpreted as being due to the influence of ion space charge in the gap on transport processes in gas [3].

According to theoretical concepts, current density at which the ion space charge essentially influences the discharge behavior is determined by the relation [2]

$$j \approx \frac{\varepsilon_0 \mu_+ U_B^2}{d_g^3}, \tag{1}$$

where ε_0 is vacuum permittivity, μ_+ is ion mobility, and d_g is gap width.

As follows from Eq. (1), shorter d_g are favorable for increasing the range of current, where the Townsend discharge can be observed. Estimates show, for example, that for a discharge in nitrogen at $d_g \leqslant 1$ mm near the minimum in the Paschen curve, the Townsend discharge must be preserved at least up to current density of 1 mA/cm^2. However, experimental data demonstrate that a stable spatially uniform state of discharge in plane-parallel short gaps is not observed in a structure with metallic electrodes even at a quite low current [4]. Instabilities in the form of filamentation of current and its oscillations are observed in such microdischarge devices [5–7].

A number of approaches are applied to stabilize the diffuse mode of a microdischarge. Examples are discharge devices of a special design, such as microhollow cathode structures [8]; structures where electrodes are covered with a dielectric layer (dielectric barrier discharge devices that operate in the ac mode) [9]; and others. The corresponding research is motivated by numerous potential applications of microdischarges, which include, among others, ultraviolet and vacuum ultraviolet light sources, sensors, microelectromechanical systems, and microreactors [10–12].

A method to obtain a stable dc Townsend discharge in a short gap is applied in a device, one electrode of which is fabricated from a high-resistivity semiconductor material [13]. Such a plane-parallel gas-discharge device is usually referred to as a semiconductor–gas-discharge (SGD) structure. As follows from this term, the structure is composed of two layers with different electronic properties. The high-resistivity electrode is usually prepared from a photoconductive semiconductor. So, the discharge current density in the device can be controlled from a light source via photoelectrical excitation of the semiconductor electrode.

The SGD devices have been initially designed for the purpose of converting infrared (IR) images into the visible light (see [13–17]). Different types of semiconductor materials, among them silicon doped with deep impurities [16,18] and semi-insulating (SI) GaAs [14,19], are utilized to fabricate photodetectors for the device. To have a high resistivity and be sensitive to the IR light, silicon photodetectors require cooling to about 100 K, while SI GaAs photodetectors can operate at the room temperature.

For the typical parameters of the SGD image converter [$d_g = 50$–100 μm and gas (Ar, N_2) pressure $p = 20$–100 hPa] discharge remains stable up to $j \approx 1$ A/cm^2 [18] (of course, pulse mode of the device operation is only possible at such a large current). The required stability of discharge in the short plane-parallel gap of the converter is provided by the negative feedback loop in the SGD structure, which tends to suppress the filamentation of current: A local increase in the discharge current density, which occurs due to a fluctuation, causes an additional local voltage drop on the high-resistivity electrode. Hence the electric field in the gap is locally reduced, which is accompanied by a decay of the fluctuation. The conditions

*yuri.astrov@mail.ioffe.ru

of suppressing current filamentation in the device for one of the mechanisms of instability of the Townsend discharge, the so-called thermal instability, were analyzed in paper [20].

According to experimental data, the stability domain of the SGD structure is quite sensitive to the discharge gap width. For example, at $d_g = 0.4$–1.0 mm, the steady state of the structure becomes unstable at a rather low current density, whose value can be as low as 100–300 μA/cm^2 [21–24]. The instability results in spatially homogeneous oscillations of discharge current in the investigated plane-parallel system [22]. These findings refer to the discharge in nitrogen at room temperature, near the minimum of the Paschen curve.

The problem of stability of low-current discharge in a device with metallic electrodes has been theoretically treated in [25] and further developed in [5,26,27]. It is supposed in these papers that the oscillatory instability of low-current dc discharges is due to the negative differential resistance (NDR) of a discharge, which is defined by the relation $R_{\rm gd} = \partial U_S/\partial i$, where i is current through the device. The value of $R_{\rm gd}$ is negative in the range of i, where an increase in current is accompanied by the decrease of voltage sustaining the discharge, U_S.

To explain the observed relatively small critical currents for the instability, a hypothesis of an essential dependence of secondary electron emission on current is advanced [5,25,26]: This effect may give rise to a rather large modulus of the NDR value at a relatively low current. As shown in the papers cited above, the discharge stability is also dependent on parameters of external circuit. Note that in traditional gas discharge experiments, electrical circuit contains lumped external elements: load resistors and capacitors. In the SGD system, the role of these elements is played by the resistance and capacitance of a semiconductor electrode. We also point out that the differential resistance of a plane-parallel gas discharge device can be defined for a square unit, as $\partial U_S/\partial j$.

A quantitative theoretical analysis of stability of SGD systems is performed in [28–31]. In these studies, the discharge region is described by the fluid approximation. The model includes continuity equations for electrons and ions, as well as the Poisson equation for potential. Processes of avalanche ionization in gas and secondary electron emission at the cathode are taken into account in the theory. The authors do not include into the model a possible dependence of secondary electron emission on the electric field (or current) in the gap. It is found that space charge of ions in the gap can lead to subcritical, supercritical, or mixed type of static current-voltage (I-V) characteristics [28]. When the I-V characteristic is a subcritical one, the spatially homogeneous stationary state is stable at a given current only in a certain range of parameters such as gap width and gas pressure. Increasing current density over a critical value $j_{\rm cr}$ causes destabilization of stationary state by a temporal mode. As a result, spatially homogeneous oscillations of harmonic or relaxation type develop.

We point out, however, that a comparison of measured values of $j_{\rm cr}$ obtained both in the current study and in previous experiments [22,23] to those calculated in the frame of model [30,31] reveals a large discrepancy between theoretical predictions and experimental data (see the Appendix). While theoretical values are in correspondence to those defined by expression (1), experimental critical currents are essentially lower. One may conclude, therefore, that effects of the ion space charge taken into account in theory [30,31] seem to be unable to explain low critical currents for emergence of oscillations.

The oscillatory instability in a planar SGD structure for discharge in nitrogen has also been theoretically treated in a recent paper [32]. The authors have considered a simplified model of dynamics and stability of Townsend discharge in the device, and were able then to reduce complicated processes there to a rather transparent description. As in [5,25,26], it is suggested that the stationary state of the system becomes unstable due to formation of NDR in the discharge gap, the effect being provided by an increase of the secondary electron emission from the cathode with the growth of current. When interpreting data of the present work, we follow the general interpretation of the instability suggested in [32].

In the context of the present experimental study it is important to stress that the authors of [32] have derived simple analytical expressions for such observables as critical current density and frequency of the self-oscillations, and their dependence on parameters of the SGD structure. These results have been obtained in approximation of small deviations from a steady state of the system (which is valid in a stable state of the structure, and for self-sustained oscillations in the vicinity of the critical state). The formulas include such parameters as discharge response time ϑ to a perturbation, negative differential resistance of discharge, $R_{\rm gd}$, and the Maxwell relaxation time of the structure, Θ. Parameter Θ determines the rate of variation of the potential difference across the discharge region. In particular, the model relates analytically transparent relationships between the mentioned parameters and critical current density for the instability. Therefore, to analyze data of the present experiments, we use the model suggested in [32].

In the current paper, we propose a method that allows one to determine both the parameter ϑ and the value of $R_{\rm gd}$ at the instability point of Townsend discharge in a short gap. The method is based on using a planar SGD system and is implemented for discharge in nitrogen in the range of discharge gap width $d_g = 0.2$–1.27 mm. Experiments are carried out at room temperature near the minimum of the Paschen curve. While the main body of data is obtained at the right-hand branch of the Paschen curve, some results refer to the left branch of the curve, also near its minimum.

Applying a high-resistivity electrode in the experimental cell provides an extended domain of gas-discharge stability. This feature of the method makes it possible to (i) get information on the dynamics of spontaneous processes for the nominally steady state of Townsend microdischarge, and (ii) investigate the critical states of such discharges. Similarly to previous experimental studies of the oscillatory behavior of SGD structures [22–24], the present work uses SI GaAs high-resistivity electrodes.

Characteristic time ϑ is determined from the discharge noise spectrum measured for the spatially uniform and nominally steady state of the structure. Values ϑ derived from experiments are compared to those suggested by the standard theory of Townsend discharge. Our study shows that observed characteristic times ϑ are much shorter of theoretical values. The magnitude $R_{\rm gd}$ can then be calculated using measured values of critical current density, characteristic time ϑ, and other parameters of the experimental system. According to obtained data, critical states of the Townsend discharge in nitrogen at the right branch of the Paschen curve occur at rather low values both of j_{cr} and $|R_{gd}|$.

II. EXPERIMENTAL DETAILS

Figure 1 shows a schematic of the experimental setup. The main parts of the device are a discharge gap, a high-resistivity semiconductor electrode, a glass plate, and a dielectric spacer. As in [22–24], a plate of SI GaAs of a thickness of $d_S = 1$ mm is used as a semiconductor electrode of the device. The spacer has a round opening that determines the diameter of the discharge volume. The gap width is defined by the thickness of the spacer. The GaAs electrode has a transparent electrical contact on its front surface that is prepared by thermal evaporation of a metal (Ni) in vacuum. The other side of the semiconductor wafer faces the gas discharge. The glass plate, which is 2 mm thick, is covered by a conducting—and transparent to the visible light—SnO_2 film that serves as a second electrode to the gas-discharge gap. This arrangement is installed into a gas-discharge chamber. In the following text, resistances and capacitances of elements of the device (including the negative differential resistance of gas-discharge region; see below) refer to 1 cm^2 of the planar structure. The chamber has two optical windows. Through one of them, the semiconductor electrode can be illuminated from an external light source. The second window can be used for the observation of the discharge glow. The chamber is equipped with a high-voltage feedthrough and a vacuum valve.

The experimental gas-discharge cell is filled with pure N_2 (99.97%) at some chosen pressure. Gas was preliminarily purified by using a trap cooled by liquid nitrogen. The pressure value is measured with CAP 100 gauge. The experiments use the high-voltage supply unit Stanford PS350. When applied voltage exceeds the gas breakdown value U_B, a discharge current flows in the device. A monitor resistor R of 10^3 Ω

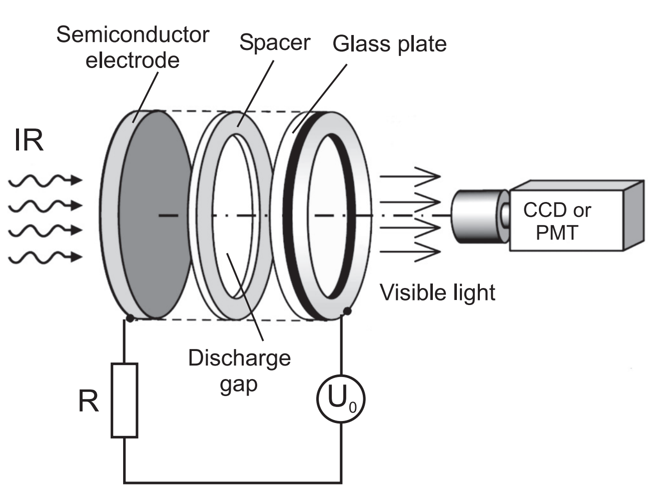

FIG. 1. Schematic presentation of the experimental setup. The discharge area is about two square centimeters. The discharge operates in the spatially homogeneous mode, as is observed with a CCD camera. A photomultiplier tube (PMT) is used to record the discharge dynamics.

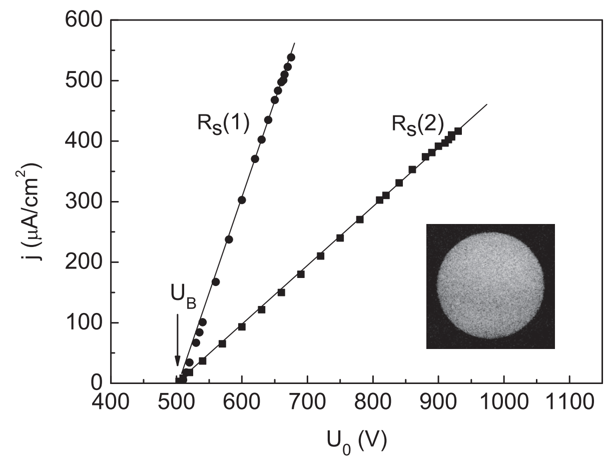

FIG. 2. I-V curves of the device measured at two resistances of a GaAs electrode. R_S values here and in the following refer to the electrode square 1 cm^2. Parameters of experiment: $p = 82$ hPa, $d_g = 0.5$ mm, $R_S(1) = 1.02 \times 10^5\ \Omega$, and $R_S(2) = 3.2 \times 10^5\ \Omega$. Sets of experimental points at $U_0 > U_B$ are approximated with straight lines. The inset is an image of gas glow in the discharge gap. The diameter of the discharge area is 15 mm.

is inserted into the electrical circuit to measure averaged in time current in the device. Both polarities of voltage can be applied to bias the studied gas-discharge structure. The value of current can be controlled by varying both the applied voltage and the intensity of IR light used to increase the conductivity of the semiconductor electrode.

In the present work, an incandescent lamp is implemented as the IR light source. A spatially homogeneous illumination of the semiconductor electrode is provided by a proper optical setup. The discharge dynamics is studied with a photomultiplier tube (PMT) that is sensitive to the light emitted from the discharge. Time series of PMT signals are recorded with an oscilloscope. The spatial distribution of discharge glow is observed with a conventional CCD camera. For experiments, we have selected electrodes exhibiting linear current-voltage (I-V) characteristics in a wide range of applied voltage. The electrodes are specified by the uniform conductivity over a wafer area. An example of typical I-V curves of the device is shown in Fig. 2. The data represent the dependencies of current density on voltage U_0 applied to electrodes of the device. In particular, Fig. 2 illustrates optical control of the structure: I-V curves are measured for two values of IR light intensity implemented to excite the semiconductor electrode. The I-V curves demonstrate that an increase in current with growing voltage in the range $U_0 > U_B$ can be approximated by linear dependencies. Figure 2 also shows an image of gas luminescence in the discharge area, where one can see the spatially homogeneous operation of the experimental structure.

Figure 3 shows Paschen curves for two cathodes, GaAs and brass, applied in the structure. Results for the GaAs electrode are obtained for two gap lengths, $d_g = 1000$ and 100 μm. The data for the brass electrode obtained in [33] at $d_g = 1000$ μm are presented here for comparison. One can see that the initiation of a breakdown in the gap does not noticeably depend

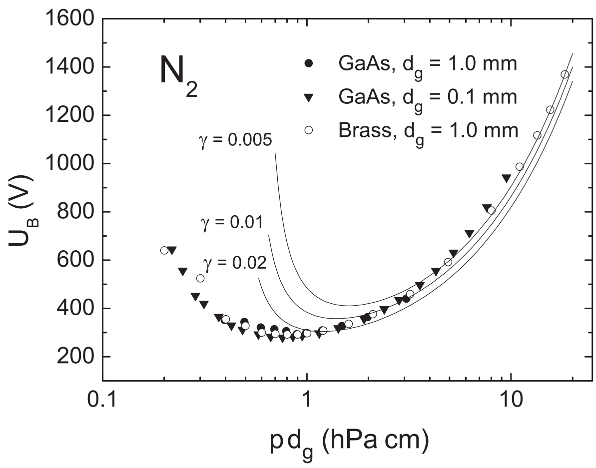

FIG. 3. Paschen curves measured in the device with cathodes fabricated from different materials (points). Shown also are theoretical dependencies calculated for different coefficients of secondary electron emission γ (see the Appendix).

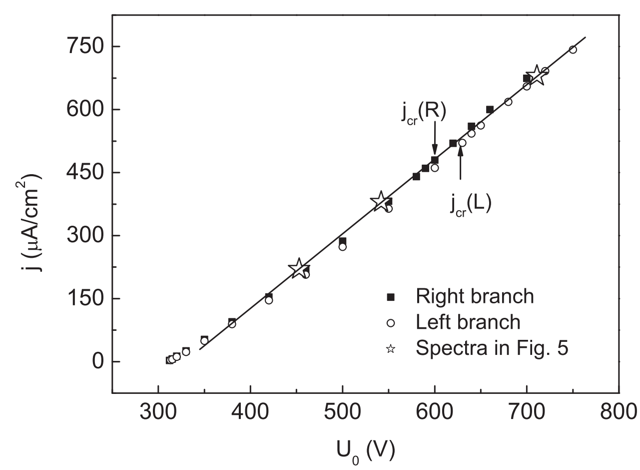

FIG. 4. I-V characteristics of the structure at $d_g = 0.25$ mm for the right ($p = 48$ hPa) and the left ($p = 18$ hPa) branches of the Paschen curve. p values are chosen to keep the same U_B values for both characteristics. Data refer to a fixed R_S value, $R_S = 6.7 \times 10^5\ \Omega$. The experimental set of points is approximated with a straight line. The arrows show $j_{\rm cr}$, at which oscillatory instability is observed; $j_{\rm cr}(R) \approx 450/\mathrm{cm}^2$, $j_{\rm cr}(L) \approx 500/\mathrm{cm}^2$. Asterisks mark current densities, at which spectra of Fig. 5 are obtained.

on the cathode material. As a consequence, the U_B value is also not dependent on the polarity of the applied voltage.

It is well known that the surface of a real or so-called "practical" cathode is always covered by a layer of unspecified contamination. As a result, secondary electron emission from a cathode is determined, to a large extent, by properties of this layer and not by the material of the cathode itself. It is established that the secondary electron emission from a metal cathode becomes sensitive to the material of the cathode only after a careful cleaning of the metal surface (see, e.g., review article [34], and further references therein). In our experiments, we have not undertaken special efforts to clean the cathodes. Therefore, surfaces of different electrodes applied in the setup seem to contain similar layers of such a contamination, which can explain the observed feature. We add to the point that, as has long been observed, the U_B value is almost independent of the cathode material at a gas pressure of about atmospheric. The reason is that secondary electron emission from a cathode may be initiated under these conditions not only by ions, but also by photons, and excited to resonance or metastable states atoms or molecules diffusing to the cathode [35].

III. REGULARITIES IN SPONTANEOUS DYNAMICS OF DISCHARGE

In this section, we study spontaneous dynamics of the SGD device in a stable steady state and transition to the oscillatory instability.

Figure 4 presents I-V characteristics of the device measured at parameters that correspond to the right- and left-hand branches of the Paschen curve, near to its minimum. The two values of p at a given d_g are chosen to give equal voltage for the gap breakdown. At obtaining both curves, R_S of the semiconductor is kept fixed. As one can see, the I-V characteristics are linear at $U_0 > U_B$; that is, $\partial j/\partial U_0 = 1/R_S =$ const. The linearity of I-V curves means that the discharge sustaining voltage U_S remains constant at varying the current density, which allows us to conclude that the Townsend mode of discharge is observed in the SGD structure [24].

Experiments show that discharge in the structure is stable in a wide range of current for both branches of the Paschen curve. However, at current density exceeding a critical value, $j_{\rm cr}$, macroscopic oscillations occur in the device. The same phenomenon of oscillatory instability was studied in [22,23] for the parameters of the SGD system close to those used in the present research.

It is instructive to investigate the dynamics of discharge in a broad range of current density, including that where the discharge is stable. Figure 5 presents frequency spectra of discharge brightness, $A(f)$, observed at different current densities. Spectra refer to the modulus of the Fourier transfom of time series for light intensity, $E(t)$, which are recorded with a photomultiplier tube. Values of current which correspond to spectra in the figure are marked on the I-V characteristic (Fig. 4) with asterisks. We stress that the data of Fig. 5 refer to the right branch of the Paschen curve. However, similar regularities of discharge dynamics are also observed in the left part of the Paschen curve. At a relatively low current (that is, in the stability domain), the spectrum of noise is specified by a maximum at a certain frequency f_0, curves 1 and 2. The f_0 value shifts to a higher frequency at the increase in current, while the band of frequencies where the amplitude of spectral components is above the background becomes more narrow. The spectral component at frequency f_0 increases sharply, curve 3, when current density reaches a certain critical value, which manifests destabilization of stationary discharge. The central noise frequency f_0 is proportional to $j^{0.5}$ in a wide range of current density (see Fig. 6), where dependence $f_0(j)$ is presented for the parameters of the experiment used to obtain the data shown in Fig. 4. We note that similar dependencies have been observed earlier for central frequency of noise

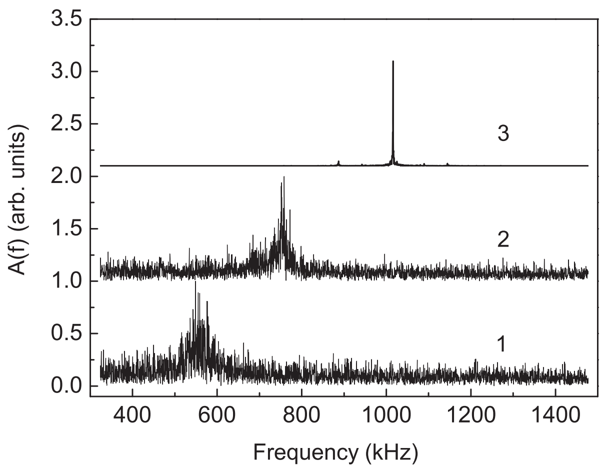

FIG. 5. Variation of frequency spectra of discharge glow at the increase in current. Data refer to different points of the I-V characteristic in Fig. 4 for the right branch of the Paschen curve. j (μA/cm^2): curve 1, 220; curve 2, 380; and curve 3, 680. Spectra are normalized to maximal values. Curves 2 and 3 are shifted in the vertical direction.

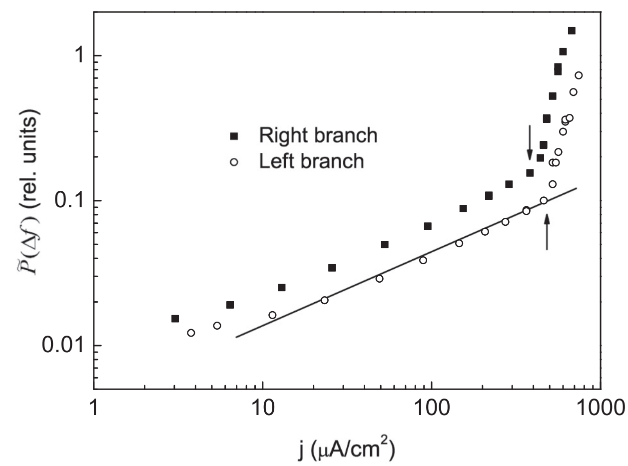

FIG. 7. Dependencies of the integral radiant power of the oscillatory component in the discharge dynamics on current density. Data refer to the right and left branches of the Paschen curve and correspond to the I-V characteristics represented in Fig. 4. The arrows mark transitions to macroscopic oscillations. The straight line represents a $j^{0.5}$ dependence.

oscillations of discharge current in the stable state of the SGD image converter [36], and in macroscopic oscillations of current in gas-discharge structures investigated in [25,26,37].

The dense frequency spectrum of discharge in the stability domain is a manifestation of random (stochastic) variation of discharge glow in time. Properties of a time series $E(t)$ can be characterized by a figure of merit that is related to the radiant power of the oscillatory component of discharge. As such a parameter, we choose in the present paper an integral of components $A(f)$ of Fourier spectrum of a time series $E(t)$, which is calculated in some frequency range Δf as follows:

$$\tilde{P}(\Delta f) = \int_{f_1}^{f_2} A(f) df. \tag{2}$$

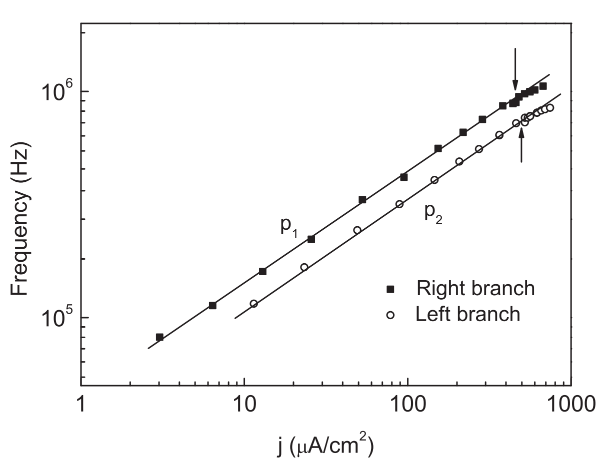

FIG. 6. Dependencies of the fundamental frequency of device on current density. Data refer to the right (p_1) and left (p_2) branches of the Paschen curve. $d_g = 0.25$ mm; $p_1 = 47$ and $p_2 = 18$ hPa; $R_S = 6.7 \times 10^5\ \Omega$. The arrows mark transitions to macroscopic oscillations.

An expansion of a series $E(t)$ in Fourier spectrum is equivalent to the presentation of the radiation source via an ensemble of oscillators of different frequency and radiant power. Thus, operation (2) gives information on the integral oscillatory power of discharge at a given band of frequencies.

Figure 7 shows an example of dependencies of $\tilde{P}(\Delta f)$ on current density in the device. The data are obtained for the frequency range $\Delta f = 5 \times 10^3$ to 2×10^6 Hz. As can be seen, $\tilde{P}(\Delta f)$ varies in proportion to $j^{0.5}$ as the current grows in the range of 2–400 μA/cm^2 in the course of voltage increase. When current density reaches the critical value, which corresponds to the instability threshold, a sharp further growth of $\tilde{P}(\Delta f)$ is observed. Values of j_{cr} are marked on the curves by arrows.

Existence of a preferential frequency in the noise spectrum of the device is a manifestation of its resonant properties. The resonance occurs due to the interaction of physical processes in the discharge region and in components of the external circuit. In general, equivalent lumped-parameter circuit of a gas-discharge device includes capacitances of the discharge gap and external circuit, on the one hand, and pseudoinductance of the discharge, on the other. The inductive behavior of discharge is due to a delay in the multiplication of carrier numbers in the gap from the variation of electric field there (see, e.g., [26,36]). The observed enhancement of the glow noise at the fundamental frequency of the oscillator (Fig. 5, curves 1 and 2) can be interpreted as being due to the response of the resonance system, which is in stable state, to the intrinsic noise of discharge [36].

The obtained data allow us to estimate quantitatively important parameters that define the properties of discharge in the investigated structure. To do this, we apply the results of paper [32] (see also [38]), where the description of dynamics of the SGD system, which is based on equations for current and voltage, is reduced to the classical equation for a nonlinear oscillator with friction. In the limit of weak damping and small deviation from the steady state, the authors derive the following expression for the resonant frequency of the system:

$$\omega_0 \approx \sqrt{\frac{\Delta}{\Theta\vartheta}}, \tag{3}$$

where

$$\Delta = \frac{U_0 - U_B}{U_B} \tag{4}$$

and

$$\Theta = \frac{\varepsilon_0\varepsilon_S}{\sigma_S}\left(1 + \frac{d_S}{\varepsilon_S d_g}\right). \tag{5}$$

Here $\omega_0 = 2\pi f_0$, time Θ determines the rate of variation of the potential difference across the discharge region (the Maxwell time of the structure), σ_S and ε_S are conductivity and dielectric constant of semiconductor material, respectively, and d_S is thickness of a semiconductor electrode. Characteristic time ϑ defines the rate of change in the number of carriers (positively charged ions) in the gap upon a deviation of the discharge voltage from its steady-state value. We point out that the higher the ratio ϑ/Θ, the larger the Q factor of the resonant structure [36].

Since values Δ and Θ are well defined in experiments, time ϑ can be found when measuring ω_0 in noise spectra (Fig. 5) and then applying Eq. (3). We define this characteristic time as the experimental one, $\vartheta_{\rm expt}$. For fixed parameters of the structure (which are d_g, p, and R_S; note that $R_S = d_S/\sigma_S$ for the square unit of the planar device), its fundamental frequency depends on current and, consequently, on parameter Δ as the square root of these variables. As a consequence, the characteristic time ϑ estimated according to Eq. (3) remains constant at a variation of current. To find $\vartheta_{\rm expt}$, we have usually analyzed the resonance frequencies of the device within the range of 100–300 kHz.

Figure 8 shows the dependence of time $\vartheta_{\rm expt}$ on the gap length determined at the fixed product $pd_g = 3.8$ cm hPa. The data are obtained from noise spectra of the device similar to those presented in Fig. 5, curves 1 and 2. That is, the measurements are made in the discharge stability domain. Figure 8 also contains corresponding data for theoretical characteristic time $\vartheta_{\rm theor}$. These are calculated using the following expression from paper [32], where it is derived in approximation of small deviations from the steady-state Townsend discharge in nitrogen:

$$\vartheta_{\rm theor} = \frac{d_g}{\mu_i E_0 k}, \tag{6}$$

where

$$k = \frac{(1+\gamma)L_y}{1 - L_y^{-1}}; \quad L_y \equiv \ln\left(\frac{1}{\gamma} + 1\right). \tag{7}$$

Here μ_i is the ion mobility which is evaluated using the relation $\mu_i p = 1550$ cm^2 hPa/(V s) from [2]. Parameter E_0 defines the intensity of avalanche ionization in the gap, $E_0 = 465\ p$ V cm^{-1} for nitrogen at the right branch of the Paschen curve. The above relationships for μ_i and E_0, where p is expressed in hPa, are taken from [2]. γ is the coefficient of secondary emission of electrons. When calculating $\vartheta_{\rm theor}$, we use $\gamma = 0.01$, of which the value is obtained from U_B observed in our experiments at given experimental conditions (see also Fig. 3 and the discussion in the Appendix). The estimated value for γ is in good correspondence to that previously determined for $T = 300\,^\circ$C [33]. In accordance with Eqs. (6) and (7), the slope of the theoretical curve in Fig. 8 is only slightly dependent on γ, which is due to the logarithmic dependence of k on γ: Variation in k is only about 50%, when γ changes in the range of 0.003–0.1.

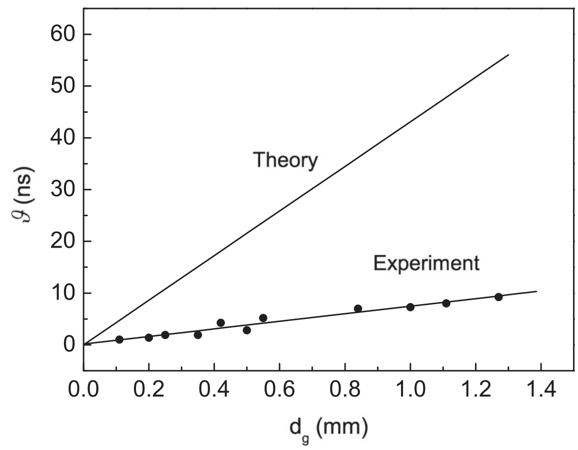

FIG. 8. Characteristic time of discharge response to perturbations as dependent on discharge gap width. Data refer to the right branch of the Paschen curve ($pd_g = 3.8$ cm hPa). The set of experimental points is obtained from observed resonance frequencies of the structure; these data are interpolated with the straight line. Theoretical dependence for ϑ is calculated using Eqs. (6) and (7) taken from [32] (see text).

Thus, it can be seen that values $\vartheta_{\rm theor}$ calculated for the right branch of the Paschen curve for discharge in nitrogen are significantly larger than experimental values. In addition, time $\vartheta_{\rm expt}$ determined for the left branch of the curve exceeds that for the right branch. This directly follows from the fact that, other conditions being equal, resonance frequency of the structure is lower for the left branch as compared to the corresponding value at the right branch of the Paschen curve (see Fig. 6).

IV. OSCILLATORY INSTABILITY AND NEGATIVE DIFFERENTIAL RESISTANCE OF DISCHARGE

According to the experimental data presented above, the oscillatory component in the discharge noise is observed in the whole range of current density, where the system is stable. In the stability domain, the relative contribution of the noise component in the discharge brightness—that is, the $\tilde{P}(\Delta f)/\bar{E}$ ratio, where $\bar{E}$ is the full discharge intensity signal—decreases with increasing current as $j^{0.5}$. [The $\bar{E}$ value is a given $E(t)$ series averaged over time.] We stress that this regularity—the decreasing role of fluctuations in the discharge with the current increase—supports the assertion that the system is stable at $j < j_{\rm cr}$. However, the absolute value of noise at the fundamental frequency ω_0 of the structure increases with the current growth, and at $j = j_{\rm cr}$, a transition to macroscopic oscillations is observed. As an example, see Fig. 5, curve 3, where the spectrum of the discharge dynamics is characterized by a narrow spectral line at the frequency ω_0. One can say therefore that spectral components of noise at the frequency

ω_0, which are observed at low currents, serve as a kind of nucleus for the oscillatory instability investigated in [22,23].

As pointed out in the Introduction, instabilities of Townsend discharges are usually explained as an effect of the NDR of discharge, $R_{\mathrm{gd}} = \partial U_S/\partial j < 0$ [5,25,27,29,32]. We also follow this generally accepted interpretation of the effect. Below, we try to estimate the NDR value in the discharge region at critical points. Using again the analogy of the SGD structure to a classical oscillator, a transition to self-sustained oscillations is observed at a state where the "friction" coefficient of the oscillator is negative. This occurs when the absolute value of R_{gd} becomes sufficiently large, so that fluctuations are no longer being damped but grow instead. According to [32], the critical current density for the oscillatory instability is

$$j_{\mathrm{cr}} = \frac{\vartheta}{\Theta}\frac{U_B}{|R_{\mathrm{gd}}|}. \quad (8)$$

In other words, the rate of fluctuations growth at the critical state, which depends on the R_{gd} value, equals the rate of their decay due to the relaxation process. The latter is determined by the Maxwell relaxation time Θ of the structure. Hence the emergence of instability for a certain prescribed Θ is favored by a small value of ϑ.

Thus, other conditions being equal, the critical current depends on the Maxwell relaxation time of a structure Θ, which in turn is determined by R_S [see Eq. (5)]. So, to find a dependence of R_{gd} on current, one can study the influence of the R_S value on j_{cr}. An example of such data is shown in Fig. 9, where j_{cr} as a function of the electrode conductance $1/R_S$ is plotted for some parameters of the discharge gap.

According to these data, a decrease in R_S is accompanied by a substantial increase in j_{cr}, which agrees qualitatively with the experimental results and theoretical considerations of [25,32]. Also, as can be seen, a rather small value of critical current is observed at large R_S. This permits studying the instability threshold in a broad range of R_S at the given d_g. We point out that the range of stable operation of the structure does not depend on the polarity of the bias voltage, which as we have shown above, is also valid for the breakdown voltage.

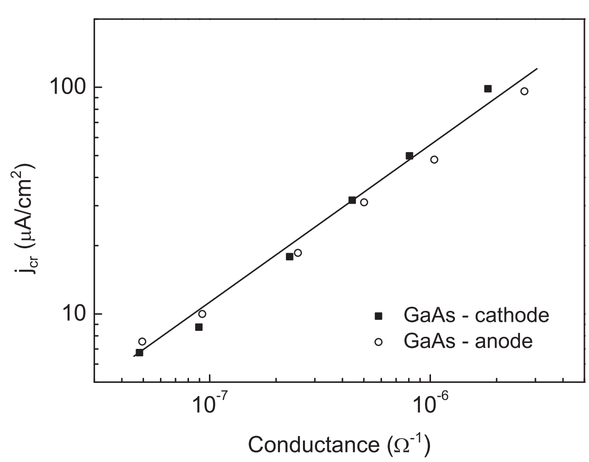

FIG. 9. Dependence of critical current density on the conductance of the semiconductor electrode for both polarities of applied voltage. Parameters of experiment: $d_g = 1.27$ mm and $p = 30$ hPa. The straight line approximates the experimental points.

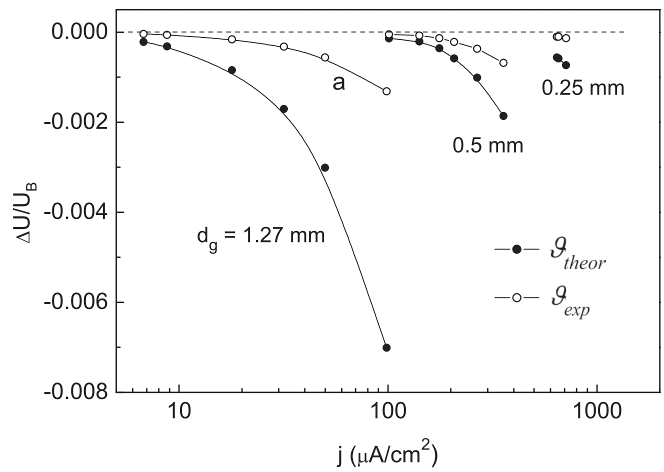

FIG. 10. I-V characteristics of the discharge region for various d_g at $pd_g = 3.8$ cm hPa (right branch of the Paschen curve). Data are normalized to $U_B = U_S(j \to 0)$. The U_B value is near 400 V (see Fig. 3). Full symbols show data calculated with θ_{theor} that are found from Eq. (6); open symbols represent results calculated with θ_{expt}, which is determined from the experimentally observed fundamental frequencies of the oscillator when applying Eq. (3).

Using Eq. (8) makes it possible to find the R_{gd} of the gap at a given j_{cr} from the experimental data for U_B, Θ, and the found value of $\vartheta_{\mathrm{expt}}$. Then, using a set of j_{cr} observed at different R_S(like that shown in Fig. 9) one can plot an I-V characteristic of discharge in the NDR region. Such a characteristic describes a multiplicity of points in the I-V plane, where the system becomes unstable at considered R_S values. The corresponding data for different d_g values, while keeping the pd_g product fixed, are shown in Fig. 10.

We stress that the oscillatory instability occurs at a relatively low value of negative differential resistance of the discharge. For instance, $|R_{\mathrm{gd}}|$ does not exceed $8 \times 10^3\ \Omega$ for the state of discharge that corresponds to curve **a** in Fig. 10. Therefore, no features in global I-V curves of the device are usually observed at an instability point (see Fig. 4).

Coming back to the results shown in Figs. 6 and 7, we remark that they are obtained at the same "electrical" parameters of the experiment (which are R_S and U_B). However, observed frequencies of oscillations and critical current densities are somewhat different. Namely, a higher j_{cr} for the left branch of the Paschen curve is observed, while the fundamental frequency of oscillations is lower there. Such behavior of the SGD structure corresponds to the general conclusion that shorter time θ (which gives a higher oscillation frequency) is in favor of lower stability of the structure.

V. CONCLUSIONS

The semiconductor–gas-discharge structure used in present experiments makes it possible to study dynamical processes in microdischarges which are responsible for their instability. The application of a high-resistivity semiconductor electrode in the planar device permits one to investigate the influence of different parameters on stability of the Townsend discharge. The method is demonstrated for the discharge in nitrogen.

Some experimental data obtained for the right branch of the Paschen curve are compared to the results of theory [30,31], where stability of SGD systems for the discharge in nitrogen is considered. The theory is based on ion space charge in the gap, which initiates the oscillatory instability. It is found that the theoretical critical current for the instability, which is estimated for a set of structure parameters, exceeds essentially the value observed in the experiment. It is concluded therefore that the ion space charge in the gap cannot be responsible for the instability at given experimental conditions.

The existence of macroscopic oscillations in the discharge current at the left branch of the Paschen curve (Figs. 4 and 7) is definitely of interest. We stress that the experimental critical current there is rather low, and comparable to that observed at the much higher pd_g product. We do not expect that a theory based on the role of ion space charge in the gap, like that developed in [31], can explain the effect. Indeed, as compared to the case of the right branch of the Paschen curve, discharge here is known to remain in the Townsend mode in a much broader range of current. Such a feature of the self-sustained discharge has been studied rather long ago (see, e.g., [39]).

The experimental data of our work are analyzed by applying the model of dynamics and stability of SGD systems, which is suggested in [32]. The authors of this paper follow early investigations, where dependence of the secondary electron emission from a cathode on discharge current is considered as a source of instability. Relatively small critical currents for oscillations observed at operation of the discharge near the minimum of the Paschen curve (including the case of the left branch of the curve) do not contradict such a model of the phenomenon. We have to point out, however, that a detailed (microscopic) mechanism of the discharge NDR for conditions of the experiments remains unclear.

One of the key parameters of the model [32] is characteristic response time ϑ of the discharge to perturbations. The value of ϑ is determined in the present work from noise spectra of the discharge. As follows from experimental data, time ϑ can be rather short at a small interelectrode distance d_g, its value being only some nanoseconds. This feature may be useful for operation of microdischarge devices, such as converters of IR images, where a high-speed performance is required [18]. It is found that characteristic times ϑ determined from experimental data are substantially shorter of theoretical values that follow from the standard concepts of dynamics of the Townsend discharge in nitrogen for the right branch of the Paschen curve.

The experimental evidence also suggests that ϑ is proportional to the width of the discharge gap. As follows from the theory, a decrease in ϑ reduces the discharge stability. However, despite the destabilizing effect of small ϑ, there is observed for short gaps an increase of range of current where the discharge remains stable. We follow in the present work the commonly accepted point of view that the effect of oscillations in a low-current dc discharge is caused by the NDR of the discharge gap, R_{gd}. Using data on the dependence of critical current on the gap width, and a theoretical approach to the problem suggested in [32], we were able to find values R_{gd} at critical points. Applying the obtained data, it has become possible to reconstruct I-V curves in the range of the NDR for the homogeneous state of discharge. When exploiting the concept of negative resistance as an origin of instability, one has to conclude that oscillations develop at a relatively small $|R_{\mathrm{gd}}|$ of the gap.

ACKNOWLEDGMENTS

We thank Yu. P. Raizer and M. S. Mokrov for helpful discussions. The study was supported by the Russian Foundation for Basic Research (Project No. 12-02-00889-a).

APPENDIX

Experimental study of the critical states of Townsend discharge, where a spontaneous transition from a spatially uniform steady state to more complex forms is observed, gives one an opportunity to test theoretical models of the discharge. Detailed theoretical consideration of stability of the Townsend discharge in the SGD systems has been recently carried out in [30,31], where a transition to the oscillating mode of discharge is investigated. Therefore, it is instructive to compare data on critical current densities, j_{cr}, observed in the present experiments, with those following from the above theory.

Results of the cited investigation are not presented via simple analytical expressions that could be used to make such a comparison directly. To determine j_{cr} predicted by the theory, one can use the bifurcation diagrams of Fig. 10 in [30]. The data include dependence of the dimensionless parameter of the system $1/\mathcal{R}_S$, at which the transition to oscillation mode occurs, on the dimensionless parameter U_t. Parameter $1/\mathcal{R}_S$ is connected to the physical resistance of the semiconductor electrode in our setup R_S, while U_t is some scaling of the physical voltage applied to electrodes of the device. Thus, the bifurcation diagram allows one to find the resistance of the electrode, at which the transition to oscillating mode (according to the theory) should be observed for a fixed supply voltage of the system. Hence the value of j_{cr} is determined, which should be expected in the frame of this theory.

The diagram is calculated for the SGD structure with the physical value of discharge gap length $d_g = 1$ mm and pressure of nitrogen $p = 41$ hPa. For comparison with the theory, we use our data obtained for $d_g = 1$ mm and $p = 38$ hPa, which is close to the parameters of the theoretical analysis. The resistance of electrode R_S related to 1 cm^2 of discharge square is $1.0 \times 10^6\,\Omega$ in the experiment. In accordance with the results shown in Fig. 11, the critical current under these conditions is $\approx 110\ \mu\mathrm{A/cm}^2$. Voltage applied to the electrodes is $U_0 \approx 600$ V, which corresponds to the theoretical dimensionless parameter $U_t = 21$.

A bifurcation diagram of [30] is calculated for a set of secondary electron emission coefficients γ, which are 0.16, 0.08, and 0.04. The value of γ in our experiments can be estimated using the observed breakdown voltage U_B (Fig. 3) and the condition for the self-sustained Townsend discharge [2]. In addition to experimental dependencies U_B (pd_g), Fig. 3 shows Paschen curves calculated at $\gamma = 0.005$, 0.01, and 0.02. An analytical approximation for the first Townsend coefficient used also in the work [32] is applied to get the curves. It is seen that the experimental data at the right branch of the Paschen curve, in the range of $pd_g = 2$–5.5 hPa cm, where the implemented analytical

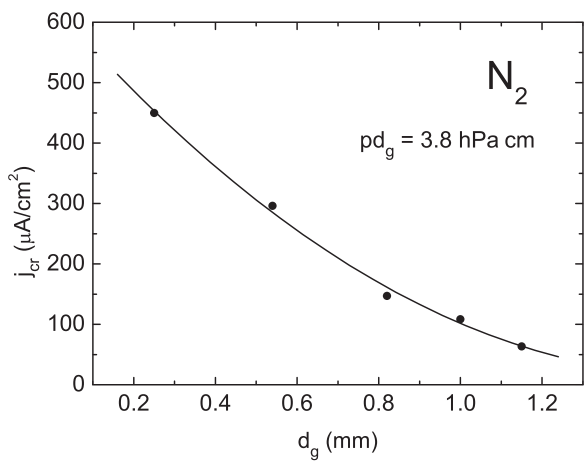

FIG. 11. Dependence of critical current density on the gap width observed at $pd_g = 3.8$ cm hPa.

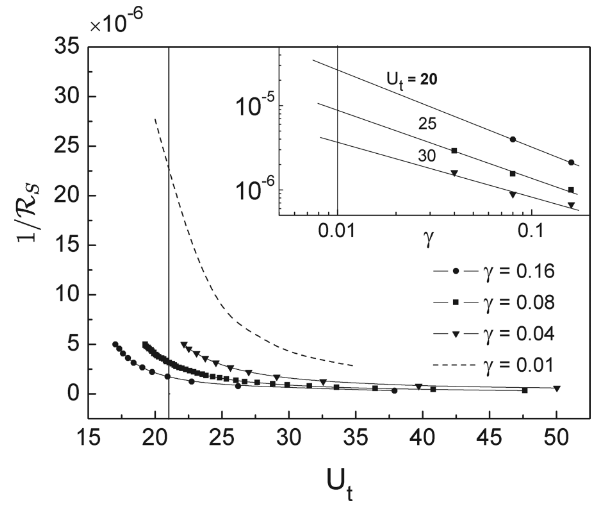

FIG. 12. Bifurcation diagram calculated for a SGD device at different values of parameter γ. Data for $\gamma = 0.04$, 0.08, and 0.16 are calculated in [30] (Fig. 10 of the cited study) for the discharge in nitrogen at $d_g = 1$ mm and $p = 41$ hPa. The dotted curve refers to the experimental conditions of the present work ($d_g = 1$ mm, $p = 38$ hPa, and $\gamma = 0.01$) and is obtained by extrapolating data of theory [30] to the case $\gamma = 0.01$. The inset demonstrates the procedure of such an extrapolation (see text).

approximation for the first Townsend coefficient is valid [2], are fitted best when using $\gamma = 0.01$.

To estimate the theoretical value of parameter $1/\mathcal{R}_S$ for conditions of the discussed experiment, we extrapolate the data [30] to the case $\gamma = 0.01$. In this regard, we note that the theoretical value of $1/\mathcal{R}_S$ plotted as a function of γ in double logarithmic scale yields a linear dependence at a fixed parameter U_t. The inset in Fig. 12 shows such presentation of data for a set of U_t. Suggesting that the observed regularity in the function $1/\mathcal{R}_S\,(\gamma)$ is (approximately) valid down to $\gamma = 0.01$, we find a theoretical value of $1/\mathcal{R}_S$ for our case. The result is illustrated by Fig. 12. Here, in addition to the bifurcation diagram from [30], the dotted line shows the curve $1/\mathcal{R}_S(U_t)$ for $\gamma = 0.01$ obtained when using the above procedure. So, we have $1/\mathcal{R}_S = 2.22 \times 10^{-5}$ at $U_t = 21$, which gives $R_S = 7.1 \times 10^4\ \Omega$ (see the intersection of the dotted and vertical lines in Fig. 12). Finally, this corresponds to $j_{\rm cr} \approx 1.7$ mA/cm^2, which exceeds the experimental value by more than an order of magnitude. One can expect that an application of theory [30] to the even smaller interelectrode distances investigated in the present work (e.g., to $d = 0.25$ mm) will also give strong disagreement with the experimental data.

[1] B. N. Klyarfeld, L. G. Guseva, and A. S. Pokrovskaya-Soboleva, Sov. Phys. Tech. Phys. **11**, 520 (1966).
[2] Yu. P. Raizer, *Gas Discharge Physics* (Springer, Berlin, 1991).
[3] L. B. Loeb, *Basic Processes of Gaseous Electronics* (University of California Press, Berkeley, 1955).
[4] Z. Lj. Petrović, N. Škoro, D. Marić, C. M. O. Mahony, P. D. Maguire, M. Radmilović-Radenović, and G. Malović, J. Phys. D: Appl. Phys. **41**, 194002 (2008).
[5] Z. Lj. Petrović and A. V. Phelps, Phys. Rev. E **47**, 2806 (1993).
[6] V. V. Osipov, Phys. Usp. **43**, 221 (2000).
[7] I. Stefanović, T. Kuschel, N. Škoro, D. Marić, Z. Lj. Petrović, and J. Winter, J. Appl. Phys. **110**, 083310 (2011).
[8] K. H. Schoenbach, A. El-Habachi, W. Shi, and M. Ciocca, Plasma Sources Sci. Technol. **6**, 468 (1997).
[9] U. Kogelschatz, Plasma Chem. Plasma Process. **23**, 1 (2003).
[10] N. Masoud, K. Martus, and K. Becker, J. Phys. D: Appl. Phys. **38**, 1674 (2005).
[11] K. H. Becker, K. H. Schoenbach, and J. G. Eden, J. Phys. D: Appl. Phys. **39**, R55 (2006).
[12] M. A. Lieberman and A. J. Lichtenberg, *Principles of Plasma Discharges and Materials Processing* (Wiley, New York, 1994).
[13] Yu. A. Astrov, V. V. Egorov, Sh. S. Kasymov, V. M. Murugov, L. G. Paritskii, S. M. Ryvkin, and Yu. N. Sheremet'ev, Sov. J. Quantum Electron. **7**, 954 (1977).
[14] Yu. A. Astrov, E. V. Beregulin, P. M. Valov, L. G. Paritskii, L. M. Portsel, S. M. Ryvkin, and O. M. Sreseli, Sov. Phys. Tech. Phys. **23**, 231 (1978).
[15] Yu. A. Astrov, H. Willebrand, L. M. Portsel, S. P. Teperick, and H.-G. Purwins, J. Appl. Phys. **74**, 2159 (1993).
[16] L. M. Portsel, Yu. A. Astrov, I. Reimann, and H.-G. Purwins, J. Appl. Phys. **81**, 1077 (1997).
[17] V. M. Murugov, A. G. Kravchenko, V. P. Lazarchuk, D. N. Litvin, V. M. Mis'ko, S. I. Petrov, A. V. Senik, and Yu. N. Sheremetiev, Proc. SPIE **4948**, 801 (2003).
[18] L. M. Portsel, Yu. A. Astrov, I. Reimann, E. Ammelt, and H.-G. Purwins, J. Appl. Phys. **85**, 3960 (1999).
[19] B. G. Salamov, A. Kh. Zeinally, N. N. Lebedeva, and L. G. Paritskii, J. Photogr. Sci. **39**, 114 (1991).
[20] Yu. A. Astrov and L. M. Portsel, Sov. Phys. Tech. Phys. **26**, 1480 (1981).
[21] B. G. Salamov, S. Ellialtioglu, B. G. Akinoglu, N. N. Lebedeva, and L. G. Patriskii, J. Phys. D: Appl. Phys. **29**, 628 (1996).

[22] C. Strümpel, Yu. A. Astrov, and H.-G. Purwins, Phys. Rev. E **62**, 4889 (2000).
[23] E. L. Gurevich, Yu. P. Raizer, and H.-G. Purwins, Tech. Phys. **51**, 180 (2006).
[24] L. M. Portsel, A. N. Lodygin, and Yu. A. Astrov, J. Phys. D: Appl. Phys. **42**, 235208 (2009).
[25] V. N. Melekhin and N. Yu. Naumov, Sov. Phys. Tech. Phys. **29**, 888 (1984).
[26] A. V. Phelps, Z. Lj. Petrović, and B. M. Jelenković, Phys. Rev. E **47**, 2825 (1993).
[27] A. A. Kudryavtsev and L. D. Tsendin, Tech. Phys. Lett. **28**, 36 (2002).
[28] D. D. Šijačić and U. Ebert, Phys. Rev. E **66**, 066410 (2002).
[29] D. D. Šijačić, U. Ebert, and I. Rafatov, Phys. Rev. E **70**, 056220 (2004).
[30] D. D. Šijačić, U. Ebert, and I. Rafatov, Phys. Rev. E **71**, 066402 (2005).
[31] D. D. Šijačić, Ph.D. thesis, Technische Universiteit Eindhoven, 2004.
[32] Yu. P. Raizer, E. L. Gurevich, and M. S. Mokrov, Tech. Phys. **51**, 185 (2006).
[33] A. N. Lodygin, L. M. Portsel, and Yu. A. Astrov, Techn. Phys. Lett. **34**, 615 (2008).
[34] A. V. Phelps and Z. Lj. Petrović, Plasma Sources Sci. Technol. **8**, R21 (1999).
[35] A. V. Phelps, Phys. Rev. **117**, 619 (1960).
[36] Yu. A. Astrov, *Dynamical Properties of Discharge Glow in the Device with Resistive Electrode* (Ioffe Physical-Technical Institute Report No. 1255, Leningrad, 1988) (in Russian).
[37] B. M. Jelenković and Z. Lj. Petrović, Jpn. J. Appl. Phys. **36**, 4728 (1997).
[38] Yu. P. Raizer and M. S. Mokrov, Phys. Plasmas **20**, 101604 (2013).
[39] A. S. Pokrovskaya-Soboleva and B. N. Klyarfeld, Sov. Phys. JETP **5**, 812 (1957).